Hindawi Publishing Corporation
Advances in Acoustics and Vibration
Volume 2013, Article ID 241025, 12 pages
http://dx.doi.org/10.1155/2013/241025

Research Article

Experimental Analysis of a Piezoelectric Energy Harvesting System for Harmonic, Random, and Sine on Random Vibration

Jackson W. Cryns, Brian K. Hatchell, Emiliano Santiago-Rojas, and Kurt L. Silvers

Health Monitoring and Radio Frequency Sensing Team, Pacific Northwest National Laboratory, P.O. Box 999, Richland, WA 99352, USA

Correspondence should be addressed to Jackson W. Cryns; cryns@uwalumni.com

Received 17 April 2013; Revised 28 June 2013; Accepted 1 July 2013

Academic Editor: K. M. Liew

Harvesting power with a piezoelectric vibration powered generator using a full-wave rectifier conditioning circuit is experimentally compared for varying sinusoidal, random, and sine on random (SOR) input vibration scenarios; the implications of source vibration characteristics on harvester design are discussed. The rise in popularity of harvesting energy from ambient vibrations has made compact, energy dense piezoelectric generators commercially available. Much of the available literature focuses on maximizing harvested power through nonlinear processing circuits that require accurate knowledge of generator internal mechanical and electrical characteristics and idealization of the input vibration source, which cannot be assumed in general application. Variations in source vibration and load resistance are explored for a commercially available piezoelectric generator. The results agree with numerical and theoretical predictions in the previous literature for optimal power harvesting in sinusoidal and flat broadband vibration scenarios. Going beyond idealized steady-state sinusoidal and flat random vibration input, experimental SOR testing allows for more accurate representation of real world ambient vibration. It is shown that characteristic interactions from more complex vibration sources significantly alter power generation and processing requirements by varying harvested power, shifting optimal conditioning impedance, inducing voltage fluctuations, and ultimately rendering idealized sinusoidal and random analyses incorrect.

1. Introduction

Modular devices requiring no external power supply have become commonplace in many industries. Every day, wireless monitors gather information on hazardous processes and remote equipment, and consumer electronics take advantage of self-contained designs. These devices are often limited in their capabilities, size, and weight by the power supply, typically electrochemical batteries. Batteries are heavy, environmentally hazardous and require regular charging or replacement. To alleviate the constraints of batteries, the power demand of the device must be reduced or external energy sources need to be implemented. Modern radio frequency sensor nodes and wireless monitors only require milliwatts (mW) of power; many drop into microwatts (μW). A growing alternative to batteries is to harness energy from the surrounding environment, a concept known as energy harvesting. Ambient energy exists in many forms including thermal energy, kinetic energy, electromagnetic radiation, and vibration. Transducers convert this environmental energy into usable electrical energy for an electrical device, effectively reducing or removing the power demand of a system [1–3]. The amount of energy that can be extracted from the environment varies greatly by application, transduction method, and processing circuitry, but many studies have shown that properly developed harvesting applications can produce ones to tens of mW of power, depending on transducer size [1, 4–8].

Vibration-powered generators are types of transducers that convert vibrational energy into electric energy. Numerous studies have been conducted on harvesting vibration energy, from powering electronics by walking [1] to charging a battery with the vibrations of a car [7]. A vibration energy harvester (VEH) incorporates both the transducer and electronics necessary to deliver power to the target electronics. Vibration transducers convert energy through

three transduction mechanisms: electrostatic transducers harness vibration energy against the electric field of a variable plate capacitor, electromagnetic transducers induct power from kinetic energy as the vibrations move a magnet, and piezoelectric transducers convert mechanical strain into a current or voltage through the piezoelectric effect [4, 7, 9]. The piezoelectric effect is the collection of charge in response to mechanical stress in certain solid materials [10]. This paper considers piezoelectric generators as they are the most compact and have the highest energy density [7, 11]. Moreover, electrostatic transducers require a separate voltage source in order to harvest energy and electromagnetic transducers typically produce voltages below 1 volt (V), making them nonideal for most applications [3, 12].

Power conditioning circuits control how the power is delivered to the electric load and come in many forms. Designs can range from just a few analog components to complex architectures controlled by firmware loaded onto microcontrollers [1, 6, 13–15]. Passive conditioning circuits contain only the components necessary to provide a DC signal at specified voltages and intervals. Other circuits utilizing nonlinear techniques like synchronous charge extraction (SCE) and synchronized switch harvesting with inductors (SSHI) make use of active circuit components such as comparators and switch controllers to maximize the extracted power. High-efficiency harvesting circuits that take advantage of extreme low power microprocessors to maximize the converted power have become commercially available.

VEHs are application-specific and require careful optimization for effective power conversion. Proper characterization of the source vibration and the transducer allows for tuning in order to achieve resonance. Much of the available literature has focused on idealized sinusoidal vibration sources, which may be due to the cross-discipline nature of the application [4–6, 8, 11, 12, 15, 16]. Unfortunately, most real-world applications incorporate broadband signals and nonlinear vibration influences that stray significantly from sinusoidal signals [17–19]. Tang et al. [8] found that SCE harvested 3.6 times the maximum power of the passive conditioning circuit and Lefeuvre et al. [4] found that the SSHI could theoretically reduce the amount of piezoelectric material needed to harvest sufficient energy by a factor of 16. Both of these studies, however, did not account for the additional power input required to implement the active control circuits. Another study [6] found that the power necessary to implement active control circuits for SCE and SSHI would be on the order of hundreds of μW, which is nonnegligible when compared to the energy harvested in nonidealized conditions [1, 6, 19]. Due to their reliance on vibration frequency, SSHI is not considered in nonsinusoidal conditions in these studies and SCE harvesting effectiveness drops significantly, in some cases was less than that of the passive conditioner [8, 17, 19].

This paper analyzes a VEH with a commercially available piezoelectric generator and a passive conditioning circuit, here referred to as the "standard circuit," and builds a relationship between vibration source characteristics and design considerations; it is organized as follows. Section 2 provides background on the theory and architecture of energy harvesting devices and information on the harvester implemented in this study. Section 3 presents the power harvesting results and design implications for sinusoidal, random, and SOR vibration sources.

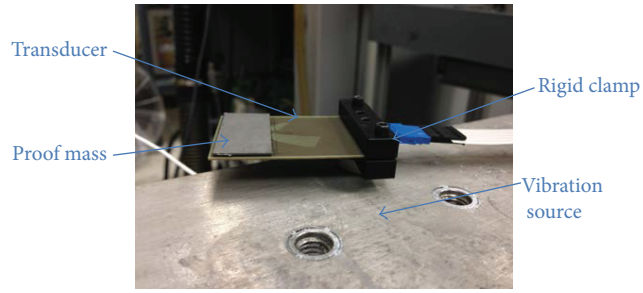

Figure 1: Transducer, proof mass, and clamping mechanism under base excitation.

2. Energy Harvesting Architecture

2.1. The Piezoelectric Generator. Materials exhibiting the piezoelectric effect have been widely developed for application as actuators. Two prominent materials have emerged, lead-zirconate-titanate (PZT) and the macrofiber composite (MFC) developed by NASA [20, 21]. Sodano et al. [7] found MFC transducers to have lower energy density and power generation than PZT. PZT conversion effectiveness is due to the high electromechanical coupling factor and modulus elasticity [5]. Raw PZT material is very brittle and resonates at frequencies significantly higher than that found in industrial application, making it difficult to implement for custom harvesters. To lower the natural frequency and increase robustness, the study [7] attached raw PZT to a much larger aluminum cantilever, which severely limits applicability. This paper assesses a commercially available Quick Pack PZT actuator as a transducer, the V25W model produced by Midé Technology Corporation [22]. The V25W forms a bimorph cantilever plate; two piezoceramic layers are bonded around a flexible dielectric center shim and between two laminate outside layers for a compact and robust transducer [23]. The transducer is mounted with a clamping mechanism rigidly attached to the vibration source. The clamp overlaps the piezoelectric material to maximize active bending stresses and thus power generation in the transducer, as seen in Figure 1.

Seismic masses are attached to the transducer to tune it to a desired natural frequency. Piezoelectric transducers have tunable frequency range due to physical limitations. Firstly, an appropriate transducer must be selected for a range of interests because the transducer cannot be tuned to a frequency higher than its bare natural frequency by adding mass. Secondly, the transducers typically have vibration displacement limitations to prevent damaging the piezoelectric material, which imposes a lower limit on the tunable frequencies. The V25W has an approximate tunable range 50 Hz to 125 Hz with a maximum peak to peak tip displacement of 0.15 in. [23]. Modal analysis techniques are used to determine

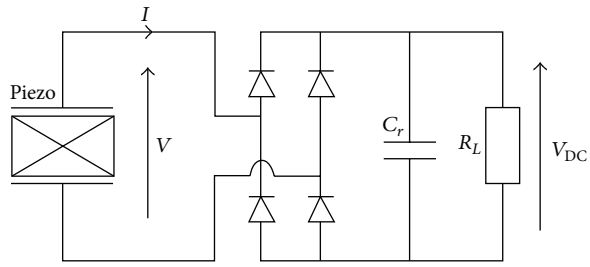

Figure 2: Standard power conditioning circuit adopted from Lefeuvre et al. [4].

the natural frequencies of the transducer for a given proof mass configuration. The analysis is conducted by providing a very short impulse from the shaker to the clamped base of the cantilever and measuring the response as the system "rings out." Without any mass, the bare transducer has a natural frequency of 124.5 Hz; in this paper, specifying a bare transducer implies a 124.5 Hz natural frequency and vice versa. Proof masses used in this study are of comparable size and weight to the generator itself, as seen in Figure 1. Since the piezoelectric material spans the entire width and length of the generator, the attachment of mass may alter the mode shape of the beam for larger displacements, thus, affecting the beam dynamics and harvested power.

2.2. Power Conditioning Circuit. Piezoelectric generators provide an alternating current (AC) signal as they oscillate in response to vibration, while microelectronics typically require direct current (DC). The standard conditioner implemented in this paper incorporates two components in parallel with the load, a full wave rectifier for current conversion and a temporary storage capacitor to smooth out the signal of the time-dependent input as shown in Figure 2. The load represents the target electronics that require power and is here considered part of the conditioning circuit. The electronic load characteristics and power demand of application define the input power needed to supply the system. Low power target circuits are often represented as purely resistive loads, although they are likely significantly more complex. The net transfer of energy is null through ideal transient circuit components such as capacitors and inductors as they do not dissipate energy. Real transient components tend to leak energy, but this loss can often be represented as a voltage drop and thus as an equivalent resistive load; diodes and transistors can similarly be modeled with equivalent resistances [24]. This study holds the load capacitance C_r constant at 110 μF and alters the resistance of a variable resistive load R_L to determine the optimum impedance and the maximum available power. Measuring the voltage across the resistor and using Ohm's law allow for calculation of the power delivered to the load, otherwise referred to as harvested power.

Devices harvesting from intermittent vibration sources like helicopters or other vehicles might not be able to supply power to the load for extended periods of time. In this case one might look to charging secondary batteries. Rechargeable batteries have varying voltage demands and can absorb varying amounts of power [25]. Rechargeable batteries follow drastically different circuit characteristics than resistors and can adapt intake current with available power. NiMH batteries have high energy density and charge around 1.2 V; however, low voltage applications are limited [26]. Other cathode compositions such as lithium and thin film solid-state batteries can continuously provide upwards of 4 V but require strict charge control circuitry [25]. Purely resistive loads allow one to find the *maximum* available power, while implementation of control components such as charge pumps, boost converters, and comparators to meet specific load demands always dissipates extra-power.

Harvesting a significant amount of the mechanical energy causes a damping effect on the electromechanical system that alters vibration amplitude [27–29]. Through the backward dynamic effects of the electromechanical system, there are optimal circuit characteristics for maximum power extraction; here we vary resistance. For instance, transducers with high electromechanical coupling factors can saturate power generation at certain impedance values, causing a dip in power generation, which can lead to more than one optimum impedance or frequency value [4, 11, 16]. Additionally, Liao et al. [11] showed that other parameters such as oscillation frequency and circuit characteristics within the transducer also affect the harvesting efficiency. Multiple equivalent circuit models for piezoelectric transducers have been developed [1, 8, 27]. The most common representation is a current source modeled in parallel with an internal capacitance and resistance. The transfer of power between interacting circuits is maximized when their equations decouple, that is, when their impedances match. For systems with varying input vibration or significant broadband characteristics, conditioning circuits that update their impedance with time could increase power conversion for deviations from optimal operating conditions [28]. However, self-updating power conditioning is out of the scope of this study.

2.3. Vibration Source. The input power for the following experimentation is provided by the LDS V721/2–PA 1000L shaker table. A closed-loop algorithm in software developed by LDS-Dactron controls the shaker table vibration. With the generator clamped and mounted to the shaker table, as seen in Figure 1, distributed dynamic inertial loads develop on the cantilever as it vibrates in response to the input forcing. A PCB Piezotronics impedance head model 288D01 measures the acceleration and force at the base of the transducer. Knowledge of these variables at the base allows for calculation of the input force when needed [30]. The VEH is tested under three different vibration signal conditions: sinusoidal, broadband, and sine tones superimposed on a broadband profile (SOR). Additionally, shock impulses will be used in modal analysis to allow for transducer tuning and parameter identification. Although purely sinusoidal vibrations are rarely seen in application, studying the response to sinusoidal input provides a starting point for harvester development and allows for model validation. Similarly, flat random vibrations are rare in application, but investigating the ability of a harvester to capture broadband vibration

similarly aides in development. Most real-world ambient vibration sources can be faithfully reproduced with a proper SOR profile, significantly aiding in harvester development for unique application.

2.4. Benchmark Theoretical Calculations. Exploitation of the piezoelectric effect as a source of electric power generation means that more mechanical strain produces more useable electrical energy. Sheets of piezoelectric material produce the largest strain when vibrating at the cantilever natural frequencies, where displacements, and thus strains, are largest. This paper considers only designing for vibration near the first natural frequency of the cantilever, which can be well modeled in one dimension [4, 29, 31, 32]. Mechanical vibration theory and the piezoelectricity constitutive equation create the following electromechanical system for the piezoelectric generator [4, 8, 17, 29, 32]:

$$F_{\text{ext}}(t) = M\ddot{x}(t) + C\dot{x}(t) + Kx(t) - k_{\text{em}}V(t), \tag{1a}$$

$$Q(t) = \kappa_p x(t) + C_p V(t), \tag{1b}$$

where M, C, and K are the modal mechanical mass, modal mechanical damping coefficient, and the modal mechanical stiffness, respectively. κ_p is the electromechanical coupling, C_p is the piezoelectric material capacitance, and $F_{\text{ext}}(t)$ is the external forcing function.

As shown in (1a) and (1b), available energy is dependent on both the induced strain and the electromechanical coupling factor. The electromechanical coupling factor is an intrinsic piezoelectric material property and a measure of conversion between electrical and mechanical energy. Ignoring the electromechanical coupling factor, κ_p, linear vibration theory allows for simple natural frequency and response displacement calculation from (1a); however, ignoring electromechanical coupling neglects backward dynamics of the VEH and would render inaccurate theoretical predictions [8]. Furthermore, deriving and simulating the responses of a unique full coupled system requires accurate knowledge of geometries and circuit characteristics within the transducer and/or the use of numerical simulation packages or numerical differential equation solvers [5, 11, 12, 16, 17, 27, 29, 32, 33].

Other studies employing various fundamental assumptions about the piezoelectric electromechanical system and input vibration have devised simpler analytical models for predicting piezoelectric power generation [4, 31, 34]. Common among almost every analytical and computational study are limiting assumptions of the external vibration, such as steady-state sinusoidal vibration and broadband vibrations of constant spectral density, which allow for simplified vibration and circuit analysis. Unfortunately, vibrations experienced in application are very rare in such convenient forms, which may compromise the validity of such calculations when applied to more complex and realistic scenarios. This study uses two approximate analytical models for benchmark comparison with experimental results, one for steady-state sinusoidal vibration and the other for flat broadband vibration.

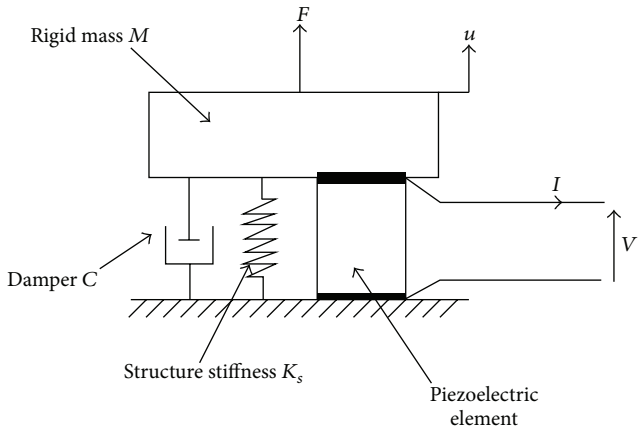

Figure 3: Simple one dimensional dynamic model for the electromenchanical system utilized by Lefeuvre et al. [4]. A similar model was used by Halvorsen [31].

Corresponding simple analytical models are not available for more complex vibration inputs such as SOR.

Lefeuvre et al. employed a one-dimensional lumped mass, spring, damper, and piezoelectric element model of the piezoelectric generators, as seen in Figure 3, to develop simple analytical formulae for harvesting capabilities under steady state harmonic vibration. Equation (2) gives the power delivered to the load (harvested power) for this model when considering the standard circuit in Figure 2. This simple model approximates the response well when considering only one mode of vibration and small (linear) displacements [4]:

$$P_{\text{sin}} = \frac{R_L \alpha^2 \omega_n^2}{\left(R_L C_0 \omega_n + \pi/2\right)} U_M^2. \tag{2}$$

C_0 and α are the internal capacitance of the piezoelectric generator and the force factor, calculated from the ratio of forcing amplitude to voltage output as described in [4], respectively. R_L, ω, and U_M are the load resistance, driving angular frequency and generator tip displacement, respectively. Even with the simplified electromechanical model, it is not unreasonable to expect the model to fit the simple sinusoidal data well at low amplitudes. In this regime, the inconsistencies between the models are minimized, such as mode shape alterations, imperfect clamp rigidity, and stray electrical losses. In general, the theoretical data is expected to be higher than measured data since the model does not account for electric losses of the bridge diodes or load capacitor.

Halvorsen derived the output power from a similar one-dimensional lumped mass, spring, damper, and piezoelectric element model when subjected to white noise [31]. This approximation is valid only in flat spectrum (constant spectral density) broadband scenarios with small displacements:

$$P_{\text{ran}} = \frac{1}{2} M S_a \frac{r \kappa_p^2 Q}{1 + \left(1/Q + \kappa_p^2 Q\right) r + r^2}. \tag{3}$$

In (3), $r = R_L \omega C_0$, M_0 is the inertial mass, and Q is the quality factor of the cantilever beam system. As in [17, 31], the modal

Table 1: System parameters.

Symbol	Representation	Value	Unit
f_n	Natural frequency	58.3^{l}; 124.5^{h}	Hz
f_a	Antiresonant frequency	60.1^{l}; 127.5^{h}	Hz
M	Modal mass	9.5^{l}; 1.1^{h}	g
Q	Quality factor	60^{l}; 120^{h}	—
α	Force factor	$4.8 * 10^{-3}$	$\mathrm{N\,V^{-1}}$
κ_p	Electromechanical coupling factor	0.92	%
C_p	Clamped capacitance	130	nf
C_r	Load capacitance	600	μf

The superscripts ^{l}, standing for low, and ^{h}, standing for high, represent the corresponding values for the frequencies near the lower and upper bounds of tunable range, 58.3 Hz and 124.5 Hz, respectively.

mass is determined as a unimorph cantilever beam with zero taper. One important difference from the model derived in [4] is that (3) is derived for a standard AC conditioning circuit, with no rectifier or filter capacitor. The calculated harvested power results in (3) are still compatible with the experimental system described in this section since the net power through the capacitor is null, save for stray electrical losses. In contrast to the harmonic model, random vibration has some inherent inconsistencies between models and they are not expected to agree as well. Parameters like modal mass and damping will alter with the dominant input frequencies, which fluctuate significantly in random vibration. Additionally, statistical variations in the input vibration from one moment to the next can lead to drastic changes in displacement amplitude and harvested power, and thus averaging is common practice [17, 19].

Due to the limited knowledge of exact internal geometries and circuit characteristics of an externally manufactured generator, all parameters necessary for experimental analysis and theoretical calculation are determined experimentally or read directly from data sheets provided by the manufacturer. With the theoretical considerations discussed herein, the electromechanical system presented in this section can be fully described at specified natural frequencies by the parameters in Table 1.

3. Vibration Source Testing and Results

This section discusses the experimental and approximate theoretical analyses of the energy harvesting architecture described in Section 2. Power is harvested by the standard circuit from a V25W piezoelectric generator subjected to varying harmonic, random, and SOR vibration scenarios.

As in most experimental applications, this paper characterizes source vibrations by acceleration in the time and frequency domains. In the following tests, input vibration amplitude refers to the input acceleration amplitude at the base. Controlling the vibration by acceleration allows for subsequent experimental validation by omitting the correction needed for input voltage variations for different shakers. However, this testing method assumes that the attachment

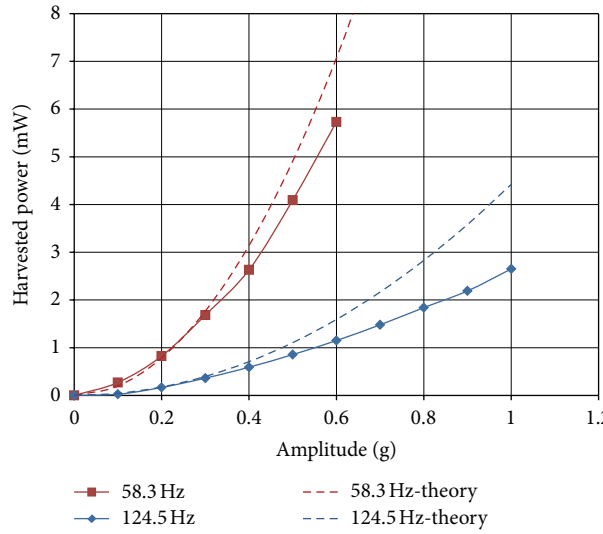

Figure 4: Theoretical and experimental harvested power as a function of sinusoidal input amplitude for two natural frequencies and constant 20 kΩ load.

of the harvester does not alter the source vibration characteristics or vice versa, which is a good assumption for shaker armatures masses and vibration sources much larger than the harvester [35]. One should also note that input power is not constant for identical acceleration amplitudes at different sinusoidal frequencies or bandwidths, but the input mechanical power is not designed against because it is of no cost to the user in application.

3.1. Harmonic Excitation. Power harvesting under steady-state harmonic excitation is tested at multiple resonant frequencies, resistance (impedance) values, and vibration amplitudes. Unless otherwise stated, the harvester is driven at the transducer natural frequency. Integration of the acceleration response, to consider displacement, reveals two important results for consideration in harvester design.

Firstly, the resulting displacement amplitude scales approximately linearly with input acceleration amplitude for a given driving frequency. This approximation applies when operating within the small transducer displacement limits. Applying Ohm's law for power through a resistor results in the harvested power scaling with the square of the input acceleration amplitude [4, 5, 27, 29]. Figure 4 shows the expected quadratic trend when tuned to 58.3 Hz and 124.5 Hz, while operating at constant load resistance, R_L = 20 kΩ. The trend at 58.3 Hz is limited to 0.6 g amplitude to avoid possibly exceeding the displacement limits and damaging the transducer. Secondly, resulting transducer tip displacement amplitude scales inversely with the square of the tuned natural frequency. Clearly, the harvested power is significantly larger at the tuned frequency than at the bare natural frequency for similar vibration amplitudes. This important result indicates that it is advantageous to tune the harvester to lower frequencies for vibration sources with multiple sine tones of similar acceleration amplitude.

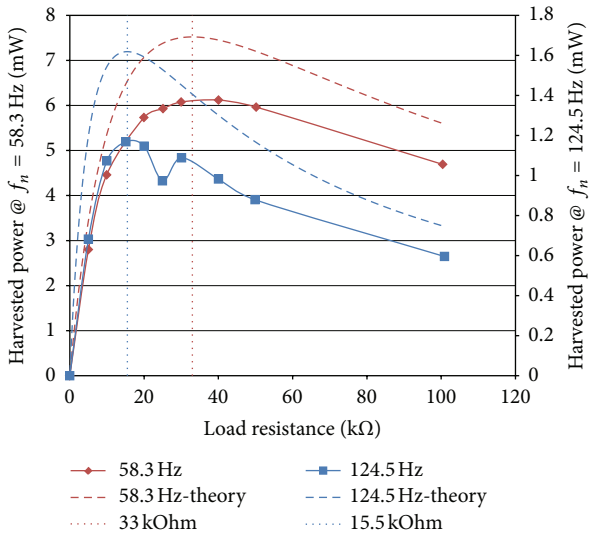

Figure 5: Harvested power as a function of load resistance for two natural frequencies at 0.6 g input amplitude.

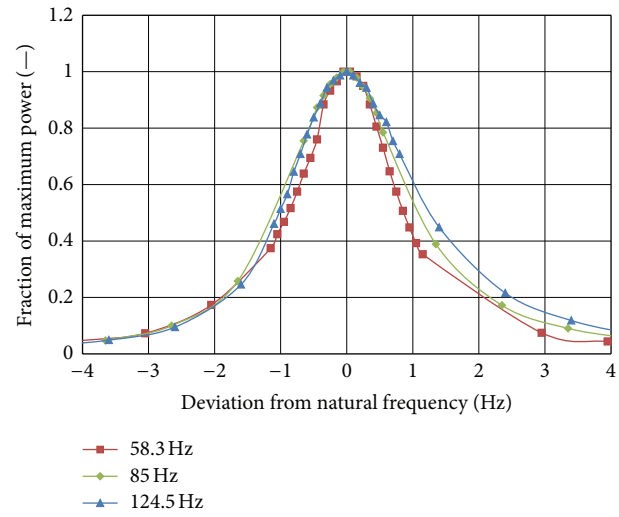

Figure 6: Harvested power FRF for three natural frequencies at optimal resistance and 0.6 g amplitude.

The theoretical model and experimental data agree well at low driving amplitudes at both frequencies. At higher amplitudes, the expected differences between the model and experimental harvested power are more evident. The theoretical power trend at 58.3 Hz has a slightly different shape than that of measured power; most consequentially, theory predicted less harvested power than was measured. Considering that the theoretical predictions should be higher than measured in all cases due to the omission of electric losses, this disagreement suggests that the approximate model derived in [4] may not be a good fit for the architecture used here.

Another important design consideration is the optimal operational resistance. Figure 5 displays harvested power versus load resistance at 0.6 g acceleration amplitude at 58.3 Hz and 124.5 Hz. Additionally, the optimal load resistances (maximum power generation) are marked vertical lines. Theoretical maximum harvested power is seen at 15.5 kΩ for the bare natural frequency and at about 33.0 kΩ for 58.3 Hz natural frequency. The optimal resistance predictions fit the experimental data well as the data reported maximum values at 15 kΩ and 40 kΩ, respectively, although the experimental resolution is quite coarse. Analytically, an inverse relation between optimal resistance and natural frequency is expected, and both findings agree [1, 11, 12, 15]. The theoretical trends provide a similar over all shape to the experimental data, but over predict harvested power by as much as 17% (approximately 1.5 mW) at 58.3 Hz and 28% (approximately 0.5 mW) at 124.5 Hz. Investing more testing time for increased resolution would be beneficial for more accurate optimal resistance determination in application.

Additionally, one will notice a dip in harvested power with optimal load resistance for the bare transducer. The drop in harvested power was seen at all vibration amplitudes is likely the saturation effect seen by Liao et al. [11] and Renno et al. [16] due to an electromechanical coupling and electrically induced mechanical damping. The absence of saturation at lower frequencies may be due to the increase in available mechanical power at lower frequencies with similar vibration amplitudes.

Figure 6 depicts the frequency response function (FRF) relative to the maximum harvested power for 58.3, 85, and 124.5 Hz natural frequencies. Deviations in driving frequency from the tuned natural frequency have a significant effect on harvested power. Generated power drops by 50% within approximately 1 Hz and 90% within approximately 3 Hz for all frequencies. This frequency dependency establishes a usable bandwidth for the transducer of just over one cycle per second, bidirectionally, outside of which power generation is severely limited. The FRF at 124.5 Hz is slightly wider on the upper limits, which suggests that the FRF becomes more generous with higher resonant frequencies but is nearly negligible in the available frequency range. The narrow FRF of the transducer reinforces the importance of accurate tuning in the design process. Theoretical data trends are not available for the frequency response function since (2) assumes that the harvester is driven at its natural frequency.

Designing for harvesting maximum power from a sinusoidal source requires weighing the gains from sine component amplitude with those from tuning to lower frequencies and finding the optimal conditioner impedance.

3.2. Random Excitation. The titles, broadband and random excitation, are often interchanged; however, random vibrations need not be broad. In application, random excitation refers to vibration inputs incorporating a finite number (dependent on resolution) of oscillation frequencies over a specified bandwidth. Naturally, random vibrations are characterized differently than sinusoidal. Most commonly, random vibrations are represented by an acceleration power spectral density (PSD) profile with units of g^2/Hz. Integrating the PSD over a frequency range and taking the square root

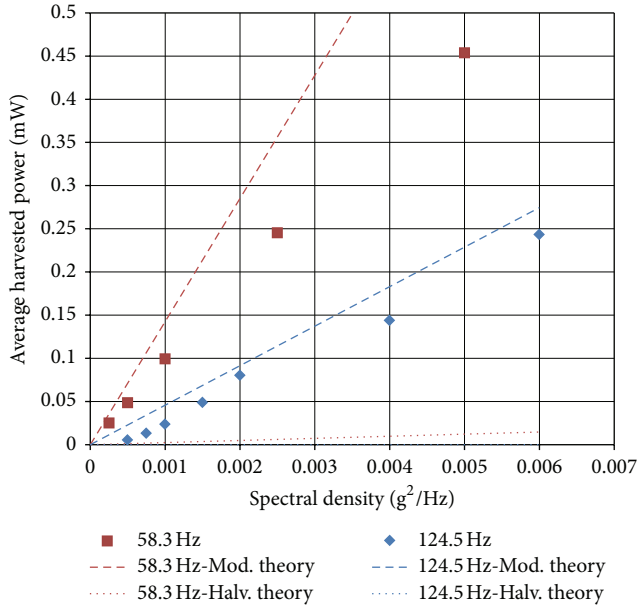

FIGURE 7: Average harvested power versus spectral density for 500 Hz bandwidth and constant 40 kΩ resistance.

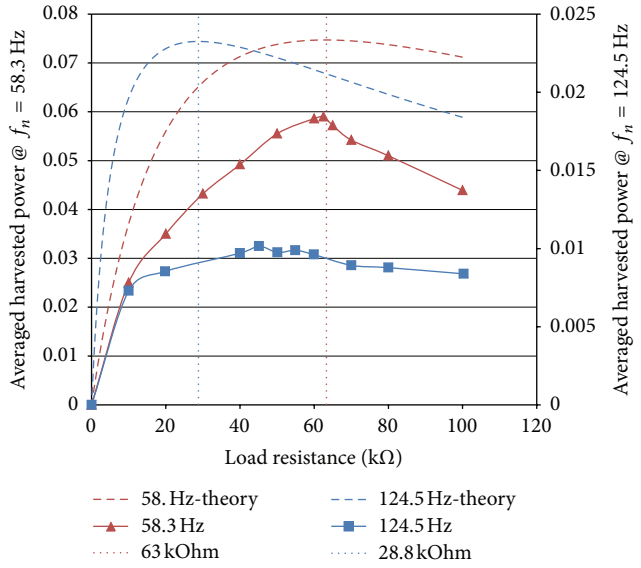

FIGURE 8: Harvested power versus load resistance for two frequencies, $S_a = 1e-3$.

result in the root mean square (RMS) level of vibration for that filtered frequency range. In this study, the harvester is subjected to PSD profiles of varying bandwidth. A new random signal, centered at the transducer natural frequency, is generated for each data point to avoid random statistical correlations. Due to statistical and time variations, harvested power is averaged over a 100-second sample for each data point to increase repeatability [17, 19].

Halvorsen [31] derived (3) as a direct formula for harvested power under white noise vibration input from properties of the generator. The term with r, κ_p, and Q in this equation is always less than or equal to one; thus, an even simpler formula for maximum power can be extracted: $P \leq 1/2mS_a$ [31]. In order to predict at least as much harvested power as was measured at $S_a = 1e-3$ (seen in Figure 7), a modal mass of at least 0.2 kg would be required at 124.5 Hz. However, such a mass is on the order one hundred times larger than the mass of the generator and proof mass, thus a scaling factor was considered for this study. The scaling factor required to predict reasonable values for harvested power increased with natural frequency. It was found that multiplying (3) by the transducer resonant frequency produced results more closely aligned to experiment. Figure 7 shows both theoretical results from (3), directly from Halvorsen, and the modified model, scaled as mentioned previously, alongside the experimental results measured when subjected to white noise at various spectral densities, set to a load resistance of 40 kΩ, and tuned to two natural frequencies. Each data point was subjected to flat spectrum random vibration with 500 Hz bandwidth.

As expected, harvested power scales linearly with spectral density, in contrast with quadratic scaling for sinusoidal vibration. The theoretical predictions from (3), represented by the dotted lines in Figure 7, are on the order of 50 and 110 times smaller than the experimental data at 58.3 Hz and 124.5 Hz, respectively, while the scaled theoretical model, represented by the dashed lines, are on the same order of magnitude. The modified model over predicts the harvested power by approximately 30% and 20% for 58.3 Hz, and 124.5 Hz respectively. This over prediction is reasonable due to the narrow resonant bandwidth of PZT piezoelectrics and the unpredictability of random vibration that lead to low harvested power.

Additionally, optimal load resistance is altered for random vibration from that of sinusoidal vibration. This variation in optimal resistance is predicted in similar theoretical derivations and seen in numerical simulations [5, 17, 19]. Figure 8 shows harvested power as a function of load resistance random excitation at the two natural frequencies. Theory predicted an optimal resistance of about 63.0 kΩ and 28.8 kΩ for 58.3 Hz and 124.5 Hz, respectively. This prediction agreed with the measured optimal resistance well at 58.3 Hz but did not agree with an approximate optimal resistance of 45 kΩ at 124.5 Hz.

Figure 9 compares harvested power at varying bandwidths for three natural frequencies. In this case, each input signal has a spectral density of 10^{-3} g^2/Hz. With constant spectral density, input power increases proportional to the square-root of the bandwidth, but this is not seen in the measured harvested power data. Except for random statistical deviations from one test point to the next [17], the harvested power remained invariant with bandwidth. We also see that the harvested power is again inversely proportional to resonant frequency. Moreover, spectral densities outside of the transducer bandwidth negligibly influence the harvested power. To illustrate this, the harvester is subjected to varying random vibration profiles that are $1e-4$ g^2/Hz near the transducer useable bandwidth of the bare transducer, as depicted in Figure 10. The harvester yielded averaged power

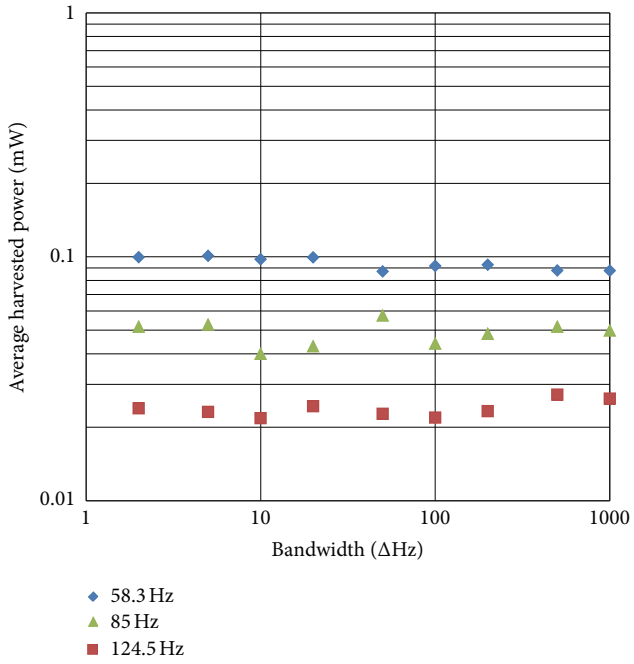

FIGURE 9: Harvested power versus bandwidth for three natural frequencies at $1e-3$ spectral density.

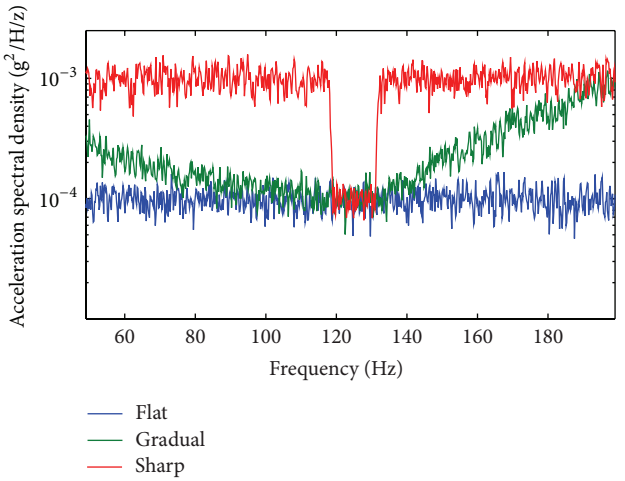

FIGURE 10: Random profiles, all centered at 124.5 Hz with $1e-4$ spectral density, with varying densities outside the transducer bandwidth.

of 0.65, 0.67, 0.71 μW, respectively, which is accounted for by statistical variations between tests [17].

In addition to low average energy conversion efficiency when compared to sinusoidal vibration, power harvesting from random or noise vibration is severely limited in application due to corresponding increases in voltage fluctuations with spectral density. Such voltage functions are not accounted for in any theoretical predictions and must be designed against in application as they can damage target electronics. Figure 11 depicts 50 second samples of voltage signal supplied to the load for varying spectral densities

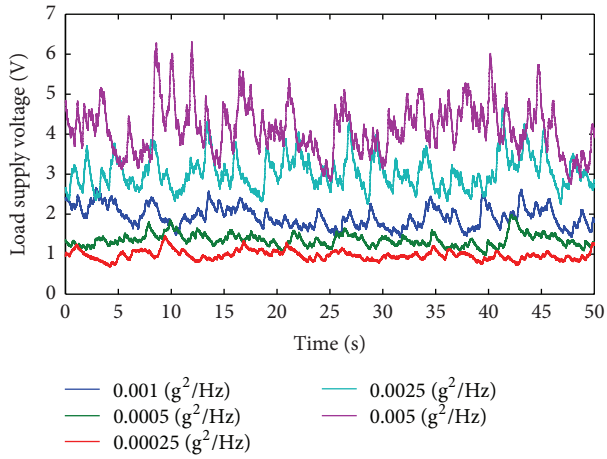

FIGURE 11: 50 second sample time responses for 500 Hz bandwidth random signals supplied to a transducer tuned to 58.3 Hz at varying spectral densities.

supplied to the transducer tuned to 58.3 Hz. Maximum to minimum voltage fluctuations increases from 0.6 V at $2.5e-4\,g^2/Hz$ to 3.5 V at $5e-3\,g^2/Hz$; above and below which, scale larger and smaller respectively. Lefeuvre et al. reported voltage fluctuations of over 10 V in order to complete a full implementation of the standard conditioner [19]. The filter capacitor in the standard circuit is able to smooth out oscillations on a small time scale; however, larger-scale changes in vibration require more attention if they were to be attenuated.

These results exhibit that the average power harvested from random vibrations is dependent only on three factors: the transducer natural frequency, the load resistance, and the spectral density near the natural frequency. In order to harvest significant power from random vibrations, rather large input vibrations are required. Moreover, the power gains are overshadowed by the implications of large load supply voltage fluctuations induced at large spectral densities. When tuned to the low end of the transducer frequency range, which produced more power, the harvester produced less than half of a milliwatt of power at a spectral density $5e{-}3\,g^2/Hz$, which is 10 to 100 time higher than ambient spectral densities seen in many industrial and vehicular applications [7, 18, 36].

3.3. Sine on Random Excitation. Purely sinusoidal or random vibrations are idealized simplifications of ambient vibration. Superposition of sinusoidal signals on broadband profiles allows for more accurate representation of environmental vibrations experienced in application like the Apache helicopter response seen in [18]. However, SOR vibration tests require control of more parameters; the driving frequency, amplitude, and number of sine tones need to be specified in addition to the random profile shape and density. Using the results of Section 2, experimental testing can be simplified. Power and voltage magnitudes scale directly with amplitude and inversely with natural frequency, and spectral densities

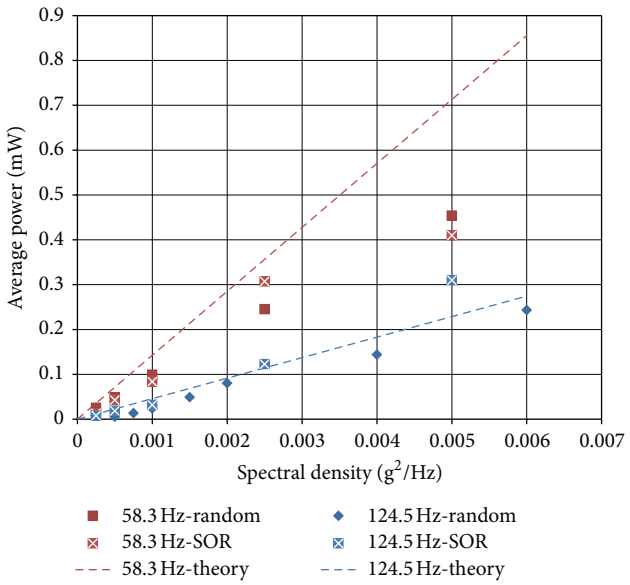

FIGURE 12: Average harvested power versus spectral density for random and SOR with sinusoidal power subtracted.

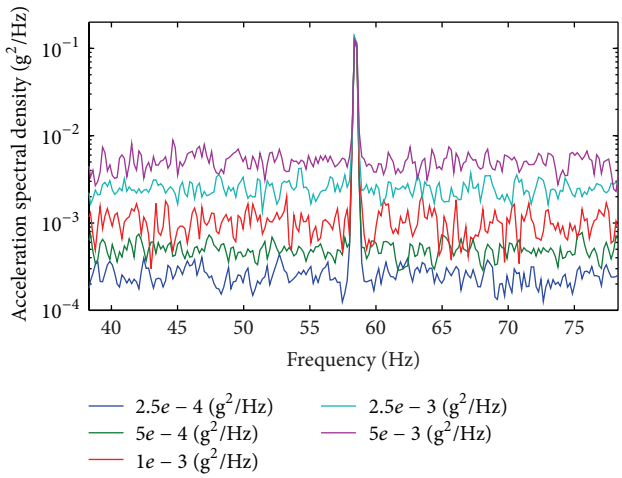

FIGURE 13: PSD of SOR input signals in Figure 17 for 58.3 Hz.

far from the transducer bandwidth negligibly influence harvesting results. A random profile is implemented flat with 150 Hz bandwidth and, as with the random vibration tests, SOR harvested power is calculated over the time average of a 100-second signal sample to increase experimental repeatability.

Driving the system with both sinusoidal and random components increases the input power within the bandwidth of the transducer, which in turn should increase the output power of the harvester. Figure 12 shows the increase in average harvested power for an SOR profile with 0.3 g sinusoidal component input and varying spectral densities against the harvested power of random vibration alone. The spectral density profiles are plotted in Figure 13. Evidently, the harvested power increases with spectral density and thus both the sinusoidal and random vibration components contribute to harvested power. Linear superposition of both components over infinite time would yield random vibration and spectral density contributions in SOR (sinusoidal power subtracted from the total power) having the same results in Figure 12: thus, theoretical calculations of harvested power from random vibration serve as a benchmark in this case as well. Time-dependent fluctuations and imperfect superposition in the control software render varying results, especially at large spectral densities. Likewise, input voltage fluctuations increase with spectral density as well. In a similar manner to Figure 11, voltage fluctuations at 58.3 Hz increase from about 0.6 V to 3.8 V as spectral density component increases from $2.5e-4\,g^2/Hz$ to $5e-3\,g^2/Hz$, which must be considered in harvester design. Altered power generation seen in these cases would be overlooked when simply ignoring the spectral content in application.

Tests conducted with varying sinusoidal component amplitudes yielded nearly identical results for increases in average power and induced voltage fluctuations, as seen previously. The significance of power gains due to spectral density, however, remains relative to the sinusoidal amplitude (i.e., a 100 μW increase in power from random content is more significant at 0.1 g than at 0.6 g sinusoid amplitude), while voltage fluctuations remain equally significant in both cases. As with harvesting from purely random vibrations, power gains from spectral content are dwarfed by the demands of induced voltage fluctuation and corresponding control circuitry power.

Sinusoidal and random vibration results revealed a gap in the dependence of optimal load resistance due to source vibration type. This variation is bridged when incorporating both sinusoidal and random components. This could further be expanded upon by incorporating nonlinear and transient inputs found in application; however, such is beyond the focus of this paper. Figure 14 shows how the optimal load resistance varies with spectral density over a constant sine component. The optimal load resistance increases with spectral density and the response shifts away from sinusoidal component dominance, until it reaches the purely random optimal load resistance. This trend suggests that the optimal resistance shift is directly dependent on the ratio of spectral density to sinusoidal component. Interactions between the two components render harmonic and random predictions of optimal resistance inaccurate for significant levels of spectral density.

Complex environmental vibration sources often compound numerous components with unique vibration signatures that result in sinusoidal components in close proximity. Flight tests for an Apache helicopter conducted in [9] show that vibrations from the main and tail rotors give dominant sine tones of similar magnitude within approximately 2 Hz of each other. The FRF for the transducer shows that interactions between sine tones sufficiently close is nonnegligible. Interactions between two nearby sine tones in the source vibration causes a significant "beating" in source vibration amplitude as the two tones go in and out of phase and also

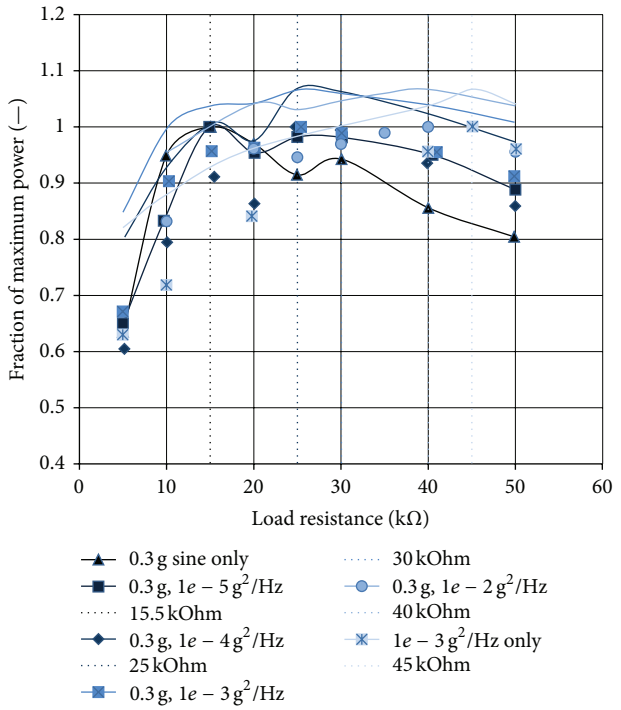

FIGURE 14: Percent of maximum harvested power within each series as a function of load resistance under sinusoidal and spectral density inputs to the bare transducer.

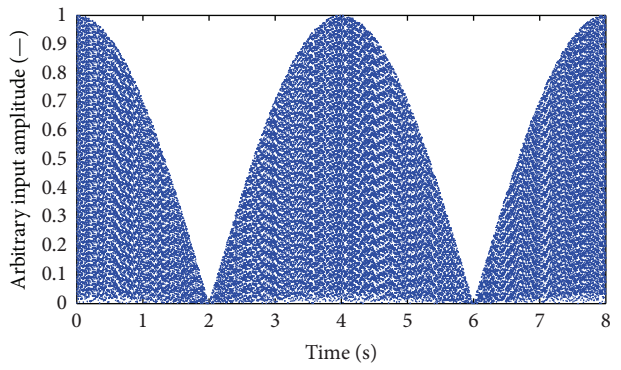

FIGURE 15: Input vibration of arbitrary acceleration units.

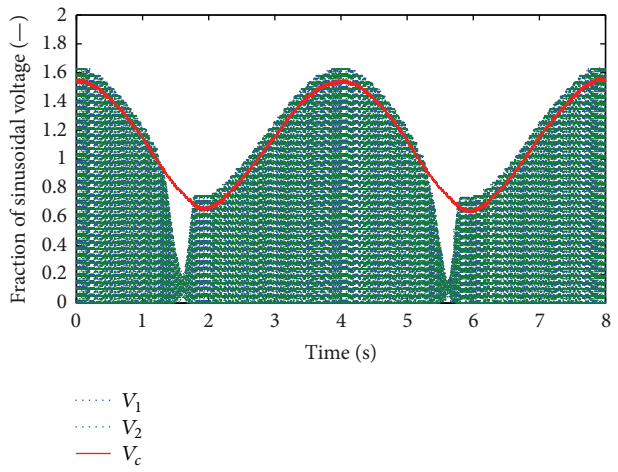

FIGURE 16: Load voltage response at 0.3 g amplitude for two sinusoidal components 0.25 Hz apart.

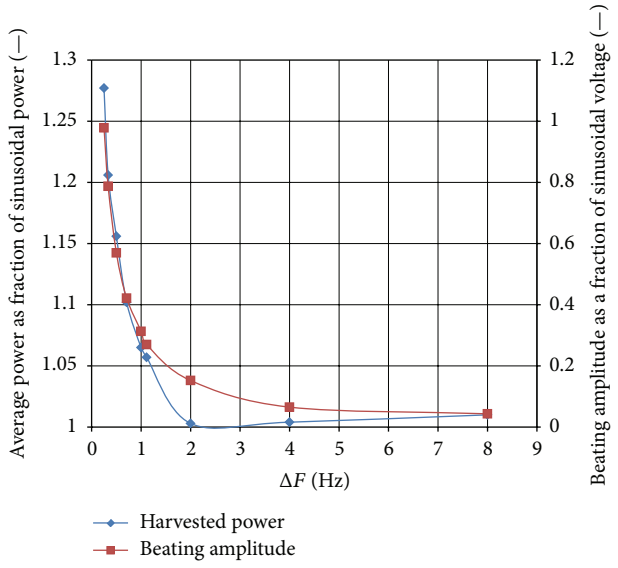

FIGURE 17: Average harvested power as a fraction of sinusoidal harvested power and beating amplitude as a fraction of sinusoidal voltage.

increase the input vibration RMS value in the bandwidth of the transducer.

Figures 15 and 16 show base input vibration and resulting load voltage waveforms experienced in the harvester, respectively, over two beating periods for two superposed sine tones of 0.3 g amplitude: one on the bare natural frequency and one 0.25 Hz above. In Figure 17, V_1 and V_2 correspond to the voltage at the transducer electrode terminals while V_c is the voltage delivered to the load. The electromechanical coupling factor alters the transducer vibration dynamics and voltage processing, resulting in nonlinear voltage waveforms delivered to the load. The charge accumulated on the capacitor prevents the voltage delivered to the load from dropping to zero as vibration drops to zero and in turn alters the piezoelectric supply voltages, V_1 and V_2. The voltage delivered to the load fluctuates by 2.61 V from crest to trough, which is just about 100% of the voltage supplied by a 0.3 g single sine tone at this natural frequency. Additionally, the average harvested power is 0.47 mW, or about 28% higher than with just a single sine tone. Assumptions of the input vibration commonly afforded to theoretical calculations and numerical simulations would not account for these results as they consider the harvester to be driven at only one frequency or a spectral content of uniform density.

The FRF of the transducer (Figure 6) indicates that beating amplitude should approach zero and harvested power should approach that of a sinusoid as the difference between the two tones increases; Figure 17 exhibits these trends. Qualitatively, as the secondary frequency recedes, its individual

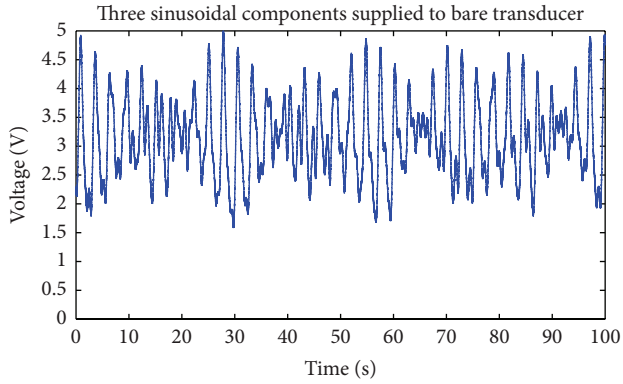

Figure 18: Resulting waveform for three unrelated sinusoidal components near the transducer natural frequency.

impact on the harvester drops with the transducer FRF; thus, the phase and spectral contributions decay. By approximately two Hz separation, the average power delivered to the load is within a few percent of that of a single sinusoid and the beating amplitude is less than 20% of the sinusoidal voltage. For this case, the peak-to-peak beating amplitude above 2 Hz separation is less than 0.35 V, which is not damaging to most electronics. However, interactions from sine tones separated by more than two Hz could become significant because both the average power delivered to the load and the beating amplitude scale directly with sinusoidal component amplitude and inversely with natural frequency.

Incorporating more sinusoidal components within the bandwidth of the transducer increases the harvested power and voltage fluctuations. Figure 18 exhibits the resulting load supply voltage waveforms for three unrelated 0.3 g sine components within the bandwidth of the transducer. In this case, the bare transducer saw voltage fluctuations of more than 3 V, which only increase in amplitude as the tuning frequency lowers. These results exemplify the results of fluctuating voltages on target electronics due to interactions of a finite number sine tones, as might be seen in complex vibration sources like the Apache helicopter [18]. As the number of sine components within a specified bandwidth increases, the vibration begins to characterize random vibrations and less orderly voltage fluctuations arise.

Harvesting power from complex vibration sources requires incorporation of more characteristic factors than idealized sinusoidal or random vibrations. As noted in Section 2, a strongly time-varying DC signal is disadvantageous and potentially damaging in application. Voltage control circuitry can be implemented to stabilize the power provided to the load at the cost of power loss. Implementing a much larger filter capacitor or additional super capacitor as storage will reduce the beating amplitude and random variations due to spectral content but at the cost of lower voltages. Power or voltage loss from implementation of additional control circuitry to maintain specified voltage requirements must be weighed against power gains of harnessing vibration from complex source vibrations. Otherwise, one can attempt to minimize such consequences by harvesting from isolated sinusoidal components with relatively low spectral content.

4. Conclusion

This paper experimentally investigated the ambient power harvesting ability of a commercially available piezoelectric vibration powered generator with a standard conditioning circuit for sinusoidal, random, and SOR excitations. Testing was conducted by characterizing the source vibration by its acceleration response, experimentally determining pertinent electrical and mechanical properties and measuring power delivered to the electric load resistor. The presented results for the idealized sinusoidal and random excitations are compared against previous theoretical predictions and numerical experiments for validation.

As was predicted analytically, the results show that lower transducer natural frequencies result in more harvested power for similar input acceleration amplitudes. Optimal load resistance varies with both natural frequency and vibration source characteristics. Vibrations with large spectral content near the transducer natural frequency induced higher average power and significant fluctuations in voltage supplied to the load. Significant voltage oscillations were also seen when multiple sinusoidal components are in close proximity.

The results presented in this paper indicate that, while useful in select cases, considering only purely sinusoidal or random vibratory environments can severely limit harvester performance in application and can bring upon unexpected and undesired consequences when applied too generally. Current theoretical and numerical simulation results are shown to predict incorrect results due to assumptions made about the input vibration and electromechanical model. The commercialization of vibration energy harvesting and application of such to complex vibration environments makes SOR testing an invaluable tool in harvester development as one can implement configurations to accurately recreate almost any ambient vibratory scenario.

Acknowledgment

This work was supported by the US Army Joint Attack Munition Systems (JAMS) Project Management Office under Interagency Agreement AGRD19D1021D1.

References

[1] P. C.-P. Chao, "Energy harvesting electronics for vibratory devices in self-powered sensors," *IEEE Sensors Journal*, vol. 11, no. 12, pp. 3106–3121, 2011.

[2] S. Roundy, E. S. Leland, J. Baker et al., "Improving power output for vibration-based energy scavengers," *IEEE Pervasive Computing*, vol. 4, no. 1, pp. 28–36, 2005.

[3] R. Want, K. I. Farkas, and C. Narayanaswami, "Energy harvesting and conservation," *IEEE Pervasive Computing*, vol. 4, no. 1, pp. 14–17, 2005.

[4] E. Lefeuvre, A. Badel, C. Richard, L. Petit, and D. Guyomar, "A comparison between several vibration-powered piezoelectric generators for standalone systems," *Sensors and Actuators A*, vol. 126, no. 2, pp. 405–416, 2006.

[5] Y. C. Shu and I. C. Lien, "Analysis of power output for piezoelectric energy harvesting systems," *Smart Materials and Structures*, vol. 15, no. 6, article 001, pp. 1499–1512, 2006.

[6] Y. K. Tan, J. Y. Lee, and S. K. Panda, "Maximize piezoelectric energy harvesting using synchronous charge extraction technique for powering autonomous wireless transmitter," in *Proceedings of the IEEE International Conference on Sustainable Energy Technologies (ICSET '08)*, pp. 1123–1128, November 2008.

[7] H. A. Sodano, D. J. Inman, and G. Park, "Comparison of piezoelectric energy harvesting devices for recharging batteries," *Journal of Intelligent Material Systems and Structures*, vol. 16, no. 10, pp. 799–807, 2005.

[8] L. Tang, Y. Yang, Y. K. Tan, and S. K. Panda, "Applicability of synchronized charge extraction technique for piezoelectric energy harvesting," in *Active and Passive Smart Structures and Integrated Systems*, vol. 7977 of *Proceedings of SPIE*, San Diego, Calif, USA, March 2011.

[9] E. O. Torres and G. A. Rincón-Mora, "Electrostatic energy harvester and Li-Ion charger circuit for micro-scale applications," in *Proceedings of the 49th Midwest Symposium on Circuits and Systems (MWSCAS '06)*, pp. 65–69, August 2007.

[10] L. Zuo, B. Scully, J. Shestani, and Y. Zhou, "Design and characterization of an electromagnetic energy harvester for vehicle suspensions," *Smart Materials and Structures*, vol. 19, no. 4, Article ID 045003, 2010.

[11] Y. Liao, Y. Lin, and H. A. Sodano, "Optimal parameters and power characteristics of piezoelectric energy harvesters with an RC circuit," in *Active and Passive Smart Structures and Integrated Systems*, vol. 7977 of *Proceedings of SPIE*, San Diego, Calif, USA, March 2011.

[12] A. Mukherjee and U. Datta, "Comparative study of piezoelectric materials properties for green energy harvesting from vibration," in *Proceedings of the Annual IEEE India Conference: Green Energy, Computing and Communication (INDICON '10)*, Kolkata, India, December 2010.

[13] C. Corporation, "EnerChip EP Universal Energy Harvester Eval Kit," 2011, http://www.cymbet.com/.

[14] J. Elmes, V. Gaydarzhiev, A. Mensah, K. Rustom, J. Shen, and I. Batarseh, "Maximum energy harvesting control for oscillating energy harvesting systems," in *Proceedings of the IEEE 38th Annual Power Electronics Specialists Conference (PESC '07)*, vol. 1–6, pp. 2792–2798, June 2007.

[15] E. Lefeuvre, A. Badel, C. Richard, and D. Guyomar, "High performance piezoelectric vibration energy reclamation," in *Smart Structures and Materials: Smart Structures and Integrated Systems*, vol. 5390 of *Proceedings of SPIE*, pp. 379–387, San Diego, Calif, USA, March 2004.

[16] J. M. Renno, M. F. Daqaq, and D. J. Inman, "On the optimal energy harvesting from a vibration source," *Journal of Sound and Vibration*, vol. 320, no. 1-2, pp. 386–405, 2009.

[17] L.-C. J. Blystad, E. Halvorsen, and S. Husa, "Piezoelectric MEMS energy harvesting systems driven by harmonic and random vibrations," *IEEE Transactions on Ultrasonics, Ferroelectrics, and Frequency Control*, vol. 57, no. 4, pp. 908–919, 2010.

[18] B. K. Hatchell, F. J. Mauss, I. A. Amaya, J. R. Skorpik, K. L. Silvers, and S. A. Marotta, "Missile captive carry monitoring and helicopter identification using a capacitive microelectromechanical systems accelerometer," *Structural Health Monitoring*, vol. 11, no. 2, pp. 213–224, 2012.

[19] E. Lefeuvre, A. Badel, C. Richard, and D. Guyomar, "Energy harvesting using piezoelectric materials: case of random vibrations," *Journal of Electroceramics*, vol. 19, no. 4, pp. 349–355, 2007.

[20] J. W. High and W. K. Wilkie, "Method of fabricating NASA-standard macro-fiber composite piezoelectric actuators," NASA, Langley Research Center, Editor 2003, http://wayback.archive-it.org/1792/20100210052417/http://hdl.handle.net/2060/20030063125.

[21] S.-N. Yun, Y.-B. Ham, and J.-H. Park, "Energy harvester using PZT actuator with a cantilver," in *Proceedings of the ICROS-SICE International Joint Conference (ICCAS-SICE '09)*, pp. 5514–5517, August 2009.

[22] M. T. Corporation, "Volture piezoelectric energy harvesters," 2010, http://www.mide.com/.

[23] M. T. Corporation, "Volture products—material properties," 2010, http://www.mide.com/.

[24] J. C. Sprott, *Introduction To Modern Electronics*, John Wiley & Sons, New York, NY, USA, 1981.

[25] M. Winter and R. J. Brodd, "What are batteries, fuel cells, and supercapacitors?" *Chemical Reviews*, vol. 104, no. 10, pp. 4245–4269, 2004.

[26] SIB Group, "VH AA, 1500 Super High Energy Series," Saft, Editor 2012.

[27] Y. Yang and L. Tang, "Equivalent circuit modeling of piezoelectric energy harvesters," *Journal of Intelligent Material Systems and Structures*, vol. 20, no. 18, pp. 2223–2235, 2009.

[28] G. K. Ottman, H. F. Hofmann, A. C. Bhatt, and G. A. Lesieutre, "Adaptive piezoelectric energy harvesting circuit for wireless remote power supply," *IEEE Transactions on Power Electronics*, vol. 17, no. 5, pp. 669–676, 2002.

[29] N. G. Stephen, "On energy harvesting from ambient vibration," *Journal of Sound and Vibration*, vol. 293, no. 1-2, pp. 409–425, 2006.

[30] C. Q. Howard, S. D. Snyder, and C. H. Hansen, "Calculation of vibratory power transmission for use in active vibration control," *Journal of Sound and Vibration*, vol. 233, no. 4, pp. 573–585, 2000.

[31] E. Halvorsen, "Energy harvesters driven by broadband random vibrations," *Journal of Microelectromechanical Systems*, vol. 17, no. 5, pp. 1061–1071, 2008.

[32] F. Lu, H. P. Lee, and S. P. Lim, "Modeling and analysis of micro piezoelectric power generators for micro-electromechanical-systems applications," *Smart Materials and Structures*, vol. 13, no. 1, pp. 57–63, 2004.

[33] A. Phipps and T. Nishida, "System modeling of piezoelectric energy harvesters," *IEEE Transactions on Power Electronics*, vol. 27, no. 2, pp. 790–802, 2012.

[34] S. R. Platt, S. Farritor, and H. Haider, "On Low-frequency electric power generation with PZT ceramics," *IEEE/ASME Transactions on Mechatronics*, vol. 10, no. 2, pp. 240–252, 2005.

[35] S. B. Han, "Analysis on natural frequency distortion due to the attachment of shaker," in *Proceedings of the 13th International Modal Analysis Conference*, vol. 1-2, pp. 1715–1721, 1995.

[36] M. A. Hassan, D. Coats, K. Gouda, Y. -J. Shin, and A. Bayoumi, "Analysis of nonlinear vibration-interaction using higher order spectra to diagnose aerospace system faults," in *Proceedings of the IEEE Aerospace Conference*, Big Sky, Mont, USA, 2012.